



Cite this: *Phys. Chem. Chem. Phys.*,  
2022, 24, 15565

# Adsorption of NO, NO<sub>2</sub> and H<sub>2</sub>O in divalent cation faujasite type zeolites: a density functional theory screening approach

Ayoub Daouli,<sup>\*ab</sup> Etienne Paul Hessou,<sup>id a</sup> Hubert Monnier,<sup>c</sup> Marie-Antoinette Dziurla,<sup>id d</sup> Abdellatif Hasnaoui,<sup>id b</sup> Guillaume Maurin,<sup>id e</sup> and Michael Badawi<sup>id \*ad</sup>

Emissions of diesel exhaust gas in confined work environments are a major health and safety concern, because of exposition to nitrogen oxides (NO<sub>x</sub>). Removal of these pollutants from exhaust gas calls for engineering of an optimum sorbent for the selective trapping of NO and NO<sub>2</sub> in the presence of water. To this end, periodic density functional theory calculations along with a recent dispersion correction scheme, namely the Tkatchenko–Scheffler scheme coupled with iterative Hirshfeld partitioning TS/HI, were performed to investigate the interactions between NO, NO<sub>2</sub>, H<sub>2</sub>O and a series of divalent cation (Be<sup>2+</sup>, Mg<sup>2+</sup>, Ca<sup>2+</sup>, Sr<sup>2+</sup>, Ba<sup>2+</sup>, Fe<sup>2+</sup>, Cu<sup>2+</sup>, Zn<sup>2+</sup>, Pd<sup>2+</sup>, and Pt<sup>2+</sup>) faujasites. This enabled the identification of the optimum zeolites to selectively capture NO<sub>x</sub> in the presence of H<sub>2</sub>O, with respect to two important criteria, such as thermodynamic affinity and regeneration. Our results revealed that Pt<sup>2+</sup> and Pd<sup>2+</sup> containing faujasites are the best candidates for effective capture of both NO and NO<sub>2</sub> molecules, which paves the way towards the use of these sorbents to address this challenging application.

Received 2nd February 2022,  
Accepted 30th May 2022

DOI: 10.1039/d2cp00553k

rsc.li/pccp

## 1. Introduction

Air quality is currently a major environmental concern. The concentration of pollutants, such as carbon oxides (CO and CO<sub>2</sub>), ozone (O<sub>3</sub>), volatile organic compounds (VOCs), nitrogen monoxide (NO) and nitrogen dioxide (NO<sub>2</sub>), released by thermal motors needs to be reduced,<sup>1,2</sup> since these chemicals are known to be highly toxic and responsible for serious health problems, *e.g.* chronic obstructive pulmonary disorder, respiratory infections and lung cancer among others.<sup>2</sup> According to the World Health Organization (WHO), 90% of the world population breathe polluted air, and seven million people die each year from diseases caused by air pollution.<sup>3</sup> Since humans spend more than 80% of their life indoors, including living and working places where pollutant levels are estimated to be typically 5 to 10 times higher than outdoor, they are particularly exposed to the typical indoor pollutants including NO, NO<sub>2</sub>, CO and VOCs.<sup>4</sup>

Along with ozone (O<sub>3</sub>), NO<sub>x</sub> (both NO and NO<sub>2</sub>) are amongst the most harmful indoor air pollutants.<sup>5</sup> NO gas is a colorless and odorless gas, while NO<sub>2</sub> is a reddish-brown gas with a strong smelly odor, and its toxicity is five times higher than that of NO.<sup>6,7</sup>

Moreover, NO<sub>x</sub> released by engines (300–1000 ppm for both NO and NO<sub>2</sub>) in a confined work environment lacking ventilation and exhaust treatment represents a major health and safety problem.<sup>8,9</sup> In France, almost 800 000 workers are exposed to such emissions. As a result, European Union regulatory requirements have attempted to address these concerns through EU Directive 2017/164, which set an occupational exposure level limit value for NO and NO<sub>2</sub> emitted from engines in a working environment of 2 and 0.5 ppm, respectively.<sup>10</sup> Therefore, the reduction of NO<sub>x</sub> emissions in exhaust gases of off-road vehicles is a current priority in occupational risk prevention. This calls for the development of efficient technologies to comply with these health standards and for improving health and safety in confined work environments.

Several strategies such as NO<sub>x</sub> storage-reduction (NSR) and selective catalytic reduction (SCR) have been proposed in the last decade, in order to limit NO<sub>x</sub> release in lean-burn engines.<sup>11–13</sup> Being efficient at high temperatures, they have already been implemented in light vehicles where the engine temperature quickly increases thanks to their continuous run. However, these techniques face several problems.<sup>14</sup> In particular,

<sup>a</sup> Laboratoire de Physique et Chimie Théoriques, CNRS, Université de Lorraine, Vandœuvre-lès-Nancy, France. E-mail: ayoub.daouli@univ-lorraine.fr, michael.badawi@univ-lorraine.fr

<sup>b</sup> LS2ME – Polydisciplinary Faculty of Khouribga – Sultan Moulay Slimane University of Beni Mellal, Khouribga, Morocco

<sup>c</sup> INRS Institut National de Recherche et de Sécurité, Vandœuvre-lès-Nancy, France

<sup>d</sup> IUT de Moselle-Est, Université de Lorraine, Saint-Avold, France

<sup>e</sup> ICGM, Université de Montpellier, CNRS, ENSCM, Montpellier, France



their efficiency for NO<sub>x</sub> reduction becomes limited in construction site machinery running discontinuously and therefore subjected to several cold starts, leading to low exhaust temperature.<sup>15</sup>

Therefore, an effective sorbent for the selective capture of low concentrations of NO and NO<sub>2</sub> in the presence of water<sup>16</sup> needs to be engineered by paying attention that residual H<sub>2</sub>O can react with NO<sub>2</sub> for producing NO and nitric acid.<sup>16,17</sup> In the context of ecological transition, adsorbent regeneration also appears crucial. Thus, a subtle balance between high selectivity and easy regeneration is required.

Recent studies revealed that inorganic sorbents such as zeolites can address the capture of NO<sub>x</sub>.<sup>17,18</sup> Indeed, on the basis of 200 existing zeolites,<sup>19–21</sup> mordenite (MOR),<sup>22,23</sup> MFI (ZSM5),<sup>24,25</sup> and faujasite (FAU) architectures have been proposed as promising candidates for NO<sub>x</sub> removal.<sup>17,26</sup> However, the identification of the most efficient zeolite in terms of topology, nature and concentration of extra-framework cations requires many experiments. To circumvent this limitation, molecular modeling is a powerful tool to narrow down the list of potential adsorbents.<sup>27,28</sup> Specifically, molecular simulations can assess accurately the adsorption energies and capacities for a large number of sorbents/sorbate pairs and therefore becomes a reliable screening tool for identifying the most efficient sorbents for the selective trapping of a target sorbate.

Herein, we present a screening approach based on density functional theory (DFT) calculations to assess the efficiency and the selectivity of zeolite materials for the target applications.<sup>29–32</sup> Typically, faujasites are good candidates for NO<sub>x</sub> trapping, thanks to the presence of the extra framework cations that can act as strong adsorption sites combined with their large supercages that enable to optimize the amount adsorbed.<sup>13,17,33,34</sup> Furthermore, the structure composition (Si/Al ratio) can be fine-tuned from one up to infinite<sup>35</sup> by modifying the hydrothermal synthesis (ratios 1 to 3) or by applying post-synthetic modifications (ratio 3 onwards).

Among this family of faujasites, the Y version<sup>36</sup> was first synthesized with a Si/Al ratio of about 2.5, exhibiting a good chemical/thermal stability and high cation exchange capacity, and therefore became industrially widely used as a molecular sieve and an adsorbent.<sup>37,38</sup> In addition, the Si/Al ratio of Y zeolites can be further increased and adjusted through stream and/or acid treatments,<sup>35</sup> yet still maintaining crystallinity. As a result, a zeolite featuring improved hydrothermal stability “Ultra Stable Y” (USY) was conceived and labeled for all structures with a Si/Al ratio of about 6 and above. Y and USY zeolites have shown remarkable promise in many industrial applications.<sup>39–41</sup>

More specifically, the objectives of the present work are to investigate the preferential adsorption configurations of NO, NO<sub>2</sub> and H<sub>2</sub>O in a series of divalent cation faujasite Y and to assess the associated interaction energies and the host/guest charge transfer. To this purpose, our periodic DFT investigations focused on a series of ten divalent cation faujasite Y (Be<sup>2+</sup>, Mg<sup>2+</sup>, Ca<sup>2+</sup>, Sr<sup>2+</sup>, Ba<sup>2+</sup>, Zn<sup>2+</sup>, Cu<sup>2+</sup>, Fe<sup>2+</sup>, Pd<sup>2+</sup> and Pt<sup>2+</sup>) with a model Si/Al ratio equal to 23. The optimal divalent cation Pt<sup>2+</sup> was further incorporated in the common zeolite Y (Si/Al = 2.4) and its adsorption behavior with respect to the 3 molecules

mentioned above was predicted to confirm the potential of this zeolite for a selective capture of NO<sub>x</sub>. The bond activation upon adsorption of the studied molecules was later analyzed to gain insight into the regeneration of these materials.

## 2. Computational and structural details

### 2.1 Structural model

Faujasite is a three-dimensional network belonging to the wide-pored zeolites (Fig. 1a). Its structure consists of 6.6 Å diameter sodalite cages (β cages) connected through hexagonal prisms (D6R) with an opening of 2.3 Å. By other windows, these β cages are connected to 12.4 Å diameter supercages (α cages) which are also linked together by a 7.4 Å diameter hexagonal window (12MR) leading to the formation of a porous network.<sup>42</sup>

The purely siliceous structure of faujasite belongs to the *Fd3m* symmetry space group,<sup>43</sup> with the standard cubic lattice

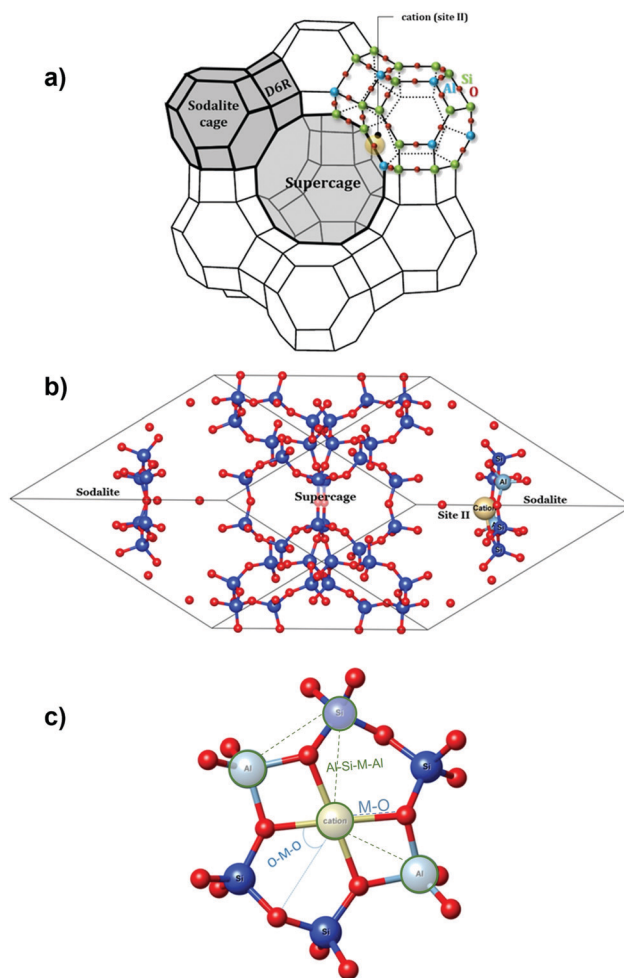


Fig. 1 (a) Scheme of the conventional cell of the faujasite with three types of cavities. The hexagonal prism (D6R), the sodalite cage (β cage) and the supercage (α cage). (b) The FAU zeolite primitive cell is displayed using balls and sticks. (c) Representation of the site II and its geometrical parameter considered during this study (i.e., the angle O–M–O).



containing 576 atoms ( $\text{Si}_{192}\text{O}_{384}$ ) and characterized by a lattice constant of 25.028 Å.<sup>44,45</sup> In the present study, to minimize computational efforts, only a 144 atom rhombohedral primitive cell was considered containing 8 hexagonal windows linking the two supercages to the sodalite cages and characterized by the following cell dimensions:  $a = b = c = 17.3432$  Å,  $\alpha = \beta = \gamma = 60^\circ$  and  $V = 3688.68$  Å<sup>3</sup>.

To obtain a Si/Al ratio equal to 23, two Si atoms were exchanged by two Al atoms in the primitive cell (Fig. 1c). Therefore, the molecular formula of the investigated cell is  $\text{M}_1\text{Al}_2\text{Si}_{46}\text{O}_{96}$ , with  $\text{M} = \text{Be}^{2+}$ ,  $\text{Mg}^{2+}$ ,  $\text{Ca}^{2+}$ ,  $\text{Sr}^{2+}$ ,  $\text{Ba}^{2+}$ ,  $\text{Zn}^{2+}$ ,  $\text{Sn}^{2+}$ ,  $\text{Fe}^{2+}$ ,  $\text{Pt}^{2+}$  or  $\text{Pd}^{2+}$ . In zeolites, the Loewenstein rule which governs Al–O interactions excludes the sharing of one oxygen atom by two  $\text{AlO}_4$  tetrahedra.<sup>46</sup> This means that the Al–O–Al bond formation is excluded from the zeolite framework and that the distance between two aluminum cations in a 6MR ( $\text{SiO}_2/\text{Al}_2\text{O}_3$ ) ring needs to be as large as possible (Fig. 1c).<sup>44</sup>

Several crystallographic investigations have shown that for a Si/Al ratio greater than five, site II (Fig. 1) is the most favorable to be occupied by cations.<sup>47,48</sup> This site is situated within the supercage, more particularly upon the hexagonal window connecting the sodalite cage to the supercage. In addition, this site is known to be accessible to most of the adsorbates.<sup>49,50</sup> Therefore, in our study, only site II was considered for the location of the different envisaged divalent cations, consistent with previous studies.<sup>51,52</sup>

## 2.2 DFT adsorption calculations

The adsorption modes and energies of  $\text{NO}_x$  and  $\text{H}_2\text{O}$  on site II of exchanged cationic zeolites were studied through periodic DFT calculations<sup>53,54</sup> using the code VASP (Vienna *Ab Initio* Simulation).<sup>55</sup> The functional of Perdew, Burke, Ernzerhof (PBE) of the generalized gradient approximation was applied (GGA).<sup>56</sup> The electron–ion interactions were described using the projector augmented plane wave (PAW) method developed by Blöchl<sup>57</sup> and adjusted later by Kresse and Joubert.<sup>58</sup> The plane wave cutoff energy was set to 450 eV and the Brillouin zone sampling at the  $\Gamma$ -point. The Kohn–Sham self-consistent total energy differences were converged within  $10^{-6}$  eV.<sup>54</sup> A 0.1 eV Gaussian smearing was applied and the atomic positions were fully relaxed until all forces were below  $0.02$  eV Å<sup>-1</sup> per atom.<sup>59</sup>

To describe the adsorption of the different guest molecules in the faujasite with a high accuracy, van der Waals (vdW) interactions have to be accounted for.<sup>60–63</sup> For this, the Tkatchenko–Scheffler scheme with iterative Hirshfeld partitioning (TS/Hi) was considered. This vdW correction method was demonstrated to accurately describe the dispersion interactions of small molecules over exchange zeolites.<sup>64</sup>

Spin-polarized (collinear) calculations were performed for all the cations.  $\text{Fe}^{2+}$  with a  $3d^6$  orbital was found to be 1.74 eV more stable in the high spin state compared to the low spin state. To further treat the strong correlation effects of Fe, the GGA + U method of Hubbard<sup>65</sup> was applied with an effective Hubbard parameter  $U_{\text{eff}}$  of 4.0.

The interaction energies between the guest molecules and the cation containing faujasites were calculated at 0 K using the following equation:

$$\Delta E_{\text{int}} = E_{(\text{FAU}+\text{guest})} - (E_{\text{FAU}} + E_{\text{guest}}) \quad (1)$$

where  $E_{\text{FAU}+\text{guest}}$  is the total energy of the zeolite with the adsorbate and  $E_{\text{FAU}}$  and  $E_{\text{guest}}$  are the total energies of the zeolite and the gaseous phase of the isolated molecule, respectively.

In a similar procedure, the dispersion force contribution  $\Delta E_{\text{disp}}$  to the interaction energy is given by

$$\Delta E_{\text{disp}} = E_{\text{disp}(\text{FAU}+\text{guest})} - E_{\text{disp}(\text{FAU})} - E_{\text{disp}(\text{guest})} \quad (2)$$

In order to further improve our understanding and to look at the effect of the interaction of the adsorbed molecule with the zeolite, both the charge density difference ( $\Delta\rho$ ) and Bader charge difference ( $\Delta Q$ ) were determined.<sup>66–68</sup>

The charge density difference can be calculated taking the superposition (obtained from the initial condition of the self-consistency cycle) of non-interacting atoms (or isolated) as the reference. The visualization of the charge density difference ( $\Delta\rho$ ) upon the adsorption of  $\text{NO}_x$  and  $\text{H}_2\text{O}$  into exchanged FAU requires three calculations as shown in the equation below:

$$\Delta\rho = \rho_{\text{FAU}+\text{guest}} - \rho_{\text{FAU}} - \rho_{\text{guest}} \quad (3)$$

where  $\rho_{\text{FAU}+\text{guest}}$  stands for the charge density of the full system,  $\rho_{\text{FAU}}$  is the charge density of the empty faujasite and  $\rho_{\text{guest}}$  is the charge density of the isolated adsorbate in the gas phase.

On the other side, the Bader approach consists of exploiting the topological properties of the charge density to partition the space in several regions, and the boundary of each Bader volume is defined as the surface through which the charge density gradient has a zero flux. Thus, the partial charge and polarization of single atoms are determined. To obtain the difference in an electronic charge  $\Delta Q$ , the following equation was used:

$$\Delta Q = Q_{\text{FAU-guest}} - (Q_{\text{FAU}} + Q_{\text{guest}}) \quad (4)$$

where  $Q_{\text{FAU-guest}}$  is the Bader charge of all the atoms upon adsorption and  $Q_{\text{FAU}}$  and  $Q_{\text{guest}}$  are the Bader charges of the clean zeolite and the isolated molecule in the gaseous phase, respectively.

## 3. Results and discussion

### 3.1. Geometry of the cation exchanged FAU zeolites

The locations of all tested cations ( $\text{M}$  = alkali metals and transition metals) in the empty and guest-loaded faujasites were determined by calculating different geometric parameters such as M–O distances (determined as the mean distance between  $\text{M}$  and the nearest 6MR oxygens), O–M–O angles (determined as the angle between the cation and two neighboring oxygens) and Al–Si–M–Al dihedral angles between  $\text{M}$  and the 6MR window plane (Fig. 1c). All distances and angles values are listed in Tables 1 and 2, respectively.



**Table 1** M–O distances (Å) of the alkaline earth metal and transition metal exchanged bare zeolites and loaded with NO, NO<sub>2</sub> and H<sub>2</sub>O

Cations	Be <sup>2+</sup>	Mg <sup>2+</sup>	Ca <sup>2+</sup>	Sr <sup>2+</sup>	Ba <sup>2+</sup>	Zn <sup>2+</sup>	Cu <sup>2+</sup>	Fe <sup>2+</sup>	Pd <sup>2+</sup>	Pt <sup>2+</sup>
Ionic Radii (pm)	45	72	100	118	135	74	73	78	86	80
Bare zeolite	1.66	2.06	2.35	2.53	2.70	1.97	2.03	2.19	2.07	2.06
NO	1.69	2.10	2.39	2.53	2.71	2.00	2.05	2.09	2.22	2.24
NO <sub>2</sub>	1.70	2.10	2.40	2.54	2.71	1.99	2.05	2.23	2.07	2.07
H <sub>2</sub> O	1.73	2.12	2.41	2.55	2.73	2.04	2.05	2.08	2.07	2.07

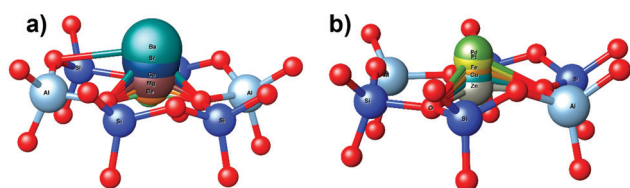
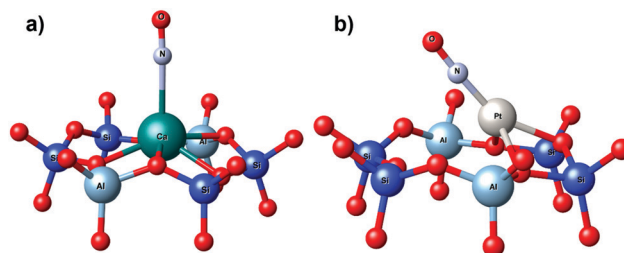
**Table 2** O–M–O angles (°) of the alkaline earth metal and transition metal exchanged bare zeolites and loaded with NO, NO<sub>2</sub> and H<sub>2</sub>O

Cations	Be <sup>2+</sup>	Mg <sup>2+</sup>	Ca <sup>2+</sup>	Sr <sup>2+</sup>	Ba <sup>2+</sup>	Zn <sup>2+</sup>	Cu <sup>2+</sup>	Fe <sup>2+</sup>	Pd <sup>2+</sup>	Pt <sup>2+</sup>
Ionic Radii (pm)	45	72	100	118	135	74	73	78	86	80
Bare zeolite	63.8	74.0	67.2	63.2	59.7	66.8	77.1	72.0	75.0	74.5
NO	65.0	72.9	67.0	63.1	59.3	67.4	67.3	69.1	71.0	70.4
NO <sub>2</sub>	64.7	73.0	66.9	63.0	59.6	67.6	76.9	70.0	74.8	74.4
H <sub>2</sub> O	67.4	72.3	66.5	62.8	59.5	65.5	76.8	71.4	75.1	74.6

**3.1.1 Bare empty faujasites.** The energy minimization of all bare empty faujasites revealed a significant increase of the dihedral angles between the cation and the 6MR windows, from 1.05° to 30.87° when going from the smallest to the biggest cation (*i.e.*, from Be<sup>2+</sup> to Ba<sup>2+</sup>). This clearly indicates that the smallest cations are positioned within the plane of the 6MR windows whereas the biggest cations are rather out of the plane as shown in Fig. 2.

Furthermore, upon increasing the cation radius from Be<sup>2+</sup> to Ba<sup>2+</sup>, we noticed an increase in the M–O distance from 1.64 Å to 2.70 Å, respectively. Moreover, a decrease in the O–M–O angle from 74.0° to 59.7° can be observed when switching from magnesium to barium. This result is in agreement with a recent work which showed that more the cations are out of the zeolite windows plane, lower are the values of the O–M–O angle.<sup>69</sup> Variations of these three geometrical parameters, in line with the ionic radius of the cation reported in Table 1, indicate that the cation position affects the interactions with the adsorbates.

Similarly, to alkaline earth metals, the relative positions of metal cations (Zn<sup>2+</sup>, Cu<sup>2+</sup>, Fe<sup>2+</sup>, Pd<sup>2+</sup> and Pt<sup>2+</sup>) within the zeolite structure were also described by the determination of the M–O distances and O–M–O angles (Tables 1 and 2). In addition, the calculations of the dihedral angles revealed values ranging from 2.5° to 5.5° which are illustrated in Fig. 2. These results clearly confirm that the most planar geometry between M and

**Fig. 2** An illustration of how the cation size influences its initial position regarding the 6MR windows plane: (a) alkaline earth family and (b) transition metal series.**Fig. 3** Illustration of the cation shift upon NO adsorption on the alkaline earth, calcium (a) and transition metal, platinum (b) zeolites.

the 6MR window is obtained with Zn<sup>2+</sup> and contradicts the fact that the cation position in the 6MR windows plane varies in the same way as its ionic radius. Similar trends were previously observed using the ZSM-5 zeolite structure.<sup>70</sup>

**3.1.2 NO, NO<sub>2</sub> and H<sub>2</sub>O loaded faujasites.** Adsorption of NO<sub>x</sub> or H<sub>2</sub>O on alkaline earth metal-exchanged zeolites induces no significant change in the position of the cations (Fig. 3a). The cations remain mostly attached to the FAU zeolite through strong covalent bonds with the nearest oxygen atoms, except for water adsorption where a slight elongation of the O–M bond (with an average of 0.05 Å) was observed (Table 1).

Determination of the O–M–O angles (Table 2) for alkaline earths showed that Be<sup>2+</sup> is the most adsorption-sensitive cation, as its corresponding angle increased from 3.6°, 1.2° and 1° after adsorption of H<sub>2</sub>O, NO and NO<sub>2</sub>, respectively.

Similar trends were also observed for transition metal exchanged zeolites. Zn<sup>2+</sup> was found to be sensitive to water as the O–M bond slightly increased from 1.95 Å to 2.04 Å (Table 1). Pt and Pd cations were found to be affected by NO adsorption as their O–M bonds significantly increased by 0.18 and 0.15 Å, respectively. In contrast to alkaline earth metals, for transition metals, the O–M–O angle decreases as the O–M bond increases, which could be due to the cation shift towards the side of the 6MR windows (near the Al atom) (Fig. 3b), while, with alkaline-earth metals, the cations remain in the 6MR windows plane (Fig. 3a).

These different geometric features of the two categories of cation–faujasites suggest distinct adsorption behavior and an associated interaction energy.

### 3.2. Energetics and iso-surface electron density

To investigate the ability of the cation exchanged FAUs to capture NO<sub>x</sub>, several adsorption modes were considered, and the most stable ones were selected (Fig. 4). Calculated energies  $\Delta E_{\text{int}}$  (kJ mol<sup>−1</sup>) together with their associated dispersion contribution  $\Delta E_{\text{disp}}$  (kJ mol<sup>−1</sup>) are reported in Table 3.

Fig. 4 shows that NO is adsorbed through its nitrogen atom, whereas NO<sub>2</sub> displays three different adsorption modes depending on whether it interacts through nitrogen or through one or two oxygen atoms. Moreover, water adsorbs preferentially through its oxygen atom although an additional interaction can occur with one of its hydrogen atoms.

#### 3.2.1 Adsorption of NO

##### 3.2.1.1 Alkaline earth metals Be<sup>2+</sup>, Mg<sup>2+</sup>, Ca<sup>2+</sup>, Sr<sup>2+</sup>, and Ba<sup>2+</sup>.

Among the three adsorbates, NO shows the weakest affinity for





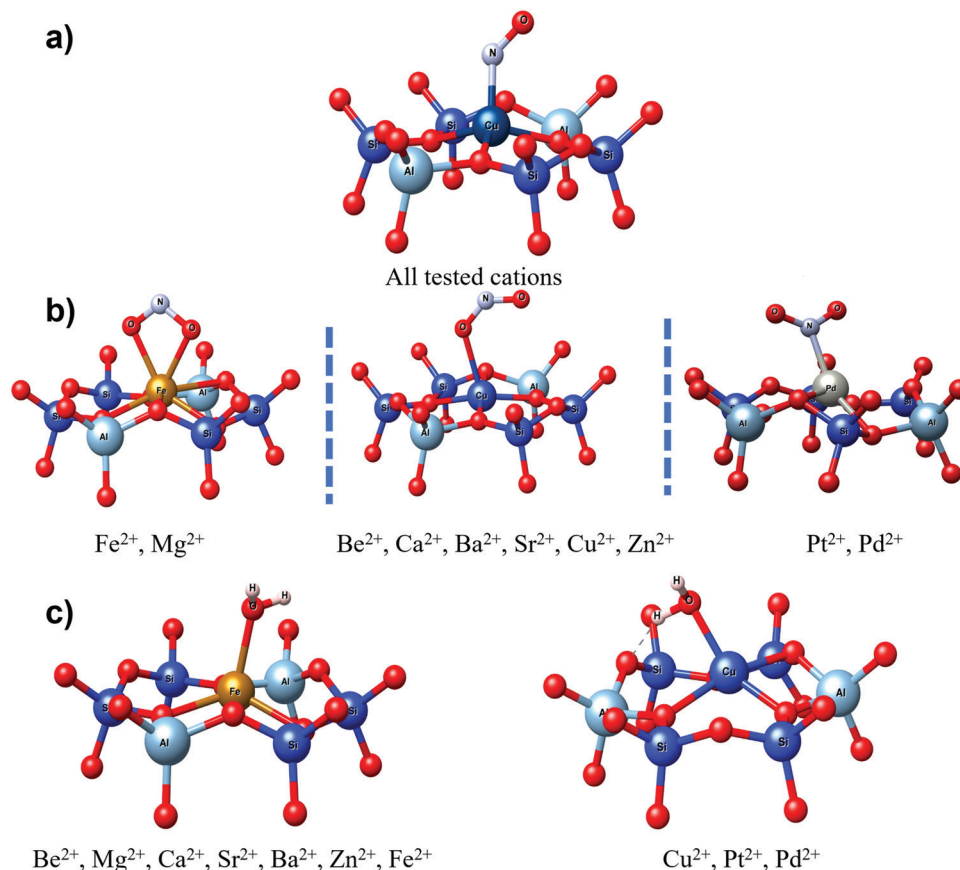


Fig. 4 Different adsorption modes for (a) NO, (b) NO<sub>2</sub> and (c) H<sub>2</sub>O in FAU exchanged with divalent cations.

**Table 3** Interaction energies  $\Delta E_{\text{int}}$  (kJ mol<sup>-1</sup>) and, in brackets, dispersion energies  $\Delta E_{\text{disp}}$  (kJ mol<sup>-1</sup>) calculated at the PBE + TS/HI theory level for NO, NO<sub>2</sub> and H<sub>2</sub>O molecules

	Be <sup>2+</sup>	Mg <sup>2+</sup>	Ca <sup>2+</sup>	Sr <sup>2+</sup>	Ba <sup>2+</sup>	Zn <sup>2+</sup>	Cu <sup>2+</sup>	Fe <sup>2+</sup>	Pd <sup>2+</sup>	Pt <sup>2+</sup>
NO	-37.6 (-11.8)	-44.5 (-10.2)	-39.0 (-10.9)	-35.0 (-11.1)	-26.6 (-10.7)	-48.7 (-10.3)	-107.8 (-9.9)	-155.5 (-9.1)	-168.7 (-16.3)	-145.6 (-15.9)
NO <sub>2</sub>	-33.8 (-16.6)	-53.2 (-12.7)	-49.9 (-13.6)	-42.4 (-12.5)	-21.8 (-12.9)	-42.1 (-13.3)	-27.2 (-14.4)	-53.7 (-14.2)	-74.2 (-13.0)	-84.7 (-15.4)
H <sub>2</sub> O	-114.8 (-10.8)	-112.0 (-7.7)	-98.9 (-8.6)	-88.7 (-8.6)	-74.6 (-7.3)	-105.3 (-9.1)	-81.6 (-8.8)	-56.3 (-9.4)	-48.2 (-19.0)	-33.2 (-16.7)

the alkaline earth metal-exchanged faujasites with a calculated interaction energy for beryllium predicted to be -37.6 kJ mol<sup>-1</sup>, including -11.8 kJ mol<sup>-1</sup> vdW contribution, *i.e.* 31% of the total interaction energy (Table 3). Furthermore, the NO interaction energy decreases progressively from -44.5 kJ mol<sup>-1</sup> with Mg<sup>2+</sup> to -26.6 kJ mol<sup>-1</sup> with Ba<sup>2+</sup>, including an average of -10 kJ mol<sup>-1</sup> vdW contribution, *i.e.* 27%. These low values indicate a decrease in the interaction force between NO and the alkaline earth series, which is correlated with an increase in the ionic radius of this group of metals. Such results indicate that increasing the electropositivity of the charge-compensating cation leads to weaker adsorption.

**3.2.1.2 Transition metals Zn<sup>2+</sup>, Fe<sup>2+</sup>, Cu<sup>2+</sup>, Pd<sup>2+</sup> and Pt<sup>2+</sup>.** The interaction energy of NO significantly increases from Zn<sup>2+</sup>

exchanged faujasite to Pt<sup>2+</sup> exchanged faujasite (Table 3). The values of the Zn<sup>2+</sup> exchanged faujasites are close to those observed for faujasites exchanged with alkaline earth metals. Higher interaction energies, such as -107.8 kJ mol<sup>-1</sup>, -155.5 kJ mol<sup>-1</sup>, -168.7 kJ mol<sup>-1</sup> and -145.6 kJ mol<sup>-1</sup>, have been calculated for Cu<sup>2+</sup>, Fe<sup>2+</sup>, Pd<sup>2+</sup> and Pt<sup>2+</sup>, respectively. The corresponding dispersion contributions are -9.9 kJ mol<sup>-1</sup>, -9.1 kJ mol<sup>-1</sup>, -16.3 kJ mol<sup>-1</sup> and -15.9 kJ mol<sup>-1</sup>, respectively, representing an average of only 7% of the total interaction energy. These results are in line with those of Kanougi *et al.*<sup>71</sup> who computed an interaction energy of -112.6 kJ mol<sup>-1</sup> for NO in ZSM-5 exchanged with Pd<sup>2+</sup>.

Similar findings were also reported by Wang *et al.*<sup>72</sup> and Sun *et al.*<sup>73</sup> for the adsorption of NO and N<sub>2</sub>O on Fe-BEA and H-BEA zeolites on the one hand, and NO and CO on Fe/ZSM-5 on the



other hand. Wang *et al.* revealed that Fe(III) exchanged BEAs show the highest affinity for NO with an interaction energy of  $-123 \text{ kJ mol}^{-1}$ , very close to the value we found for Fe(II)-FAU. However, Sun *et al.* obtained a much higher energy of  $-258 \text{ kJ mol}^{-1}$  for the ZSM-5 exchanged with Fe(II) most probably due to the location of the Fe(II) on the 8MR site. Many studies reported that cations located in the 8MR sites lead to higher interaction energies compared to the cations located in the 6MR site.<sup>74,75</sup> Furthermore, these previous studies revealed that, in all investigated zeolites, NO molecules preferentially adsorb *via* their nitrogen rather than their oxygens, in agreement with our findings reported in Fig. 4.

Fig. 5 represents the negative and positive iso-surfaces between Ba-NO and Pt-NO. The high electrostatic interactions between nitrogen and Pt<sup>2+</sup> were confirmed through the high charge transfer, together with the Bader method based computed  $\Delta Q$  (0.14 e;  $-0.17 \text{ e}$ ) for Pt and N, respectively. It is not the case with the Ba cation where its Bader charge was almost unaffected by the adsorption of NO. The calculated distance between the Pt atom and N atom of NO ( $d_{\text{Pt-N}} = 1.92 \text{ \AA}$ ) confirmed this result, indicating a chemical bond formation between the cations and the nitrogen atom of NO, with the formation of complexes.<sup>76,77</sup>

### 3.2.2 Adsorption of NO<sub>2</sub>

#### 3.2.2.1 Alkaline earth metals Be<sup>2+</sup>, Mg<sup>2+</sup>, Ca<sup>2+</sup>, Sr<sup>2+</sup>, and Ba<sup>2+</sup>.

The NO<sub>2</sub> interaction energy varies between  $-53.2 \text{ kJ mol}^{-1}$  and  $-21.8 \text{ kJ mol}^{-1}$  from Mg<sup>2+</sup> to Ba<sup>2+</sup> (Table 3). This relatively weak interaction is in line with the absence of the charge transfer between Ba<sup>2+</sup> and NO<sub>2</sub> (Fig. 6a). The significant decrease of the interaction energy along this family of cations follows the decrease in the hardness of the cation, leading to a weaker interaction with hard base molecules, *i.e.* HSAB theory (Hard Soft Bases and Acids) introduced by Parr Pearson.<sup>78</sup>

3.2.2.2 Transition metals Zn<sup>2+</sup>, Fe<sup>2+</sup>, Cu<sup>2+</sup>, Pd<sup>2+</sup> and Pt<sup>2+</sup>. For faujasites exchanged with transition metals, Table 3 shows that NO<sub>2</sub> is less strongly adsorbed as compared with NO and preferentially interacts through its oxygen atoms for most of the cations as shown in Fig. 4b. The total interaction energy reaches a maximum of  $-53.7 \text{ kJ mol}^{-1}$  for Fe<sup>2+</sup>, which is similar to the value observed for Mg<sup>2+</sup> ( $-53.2 \text{ kJ mol}^{-1}$ ), reflecting the same interaction mode of NO<sub>2</sub> with these two cations. Zinc

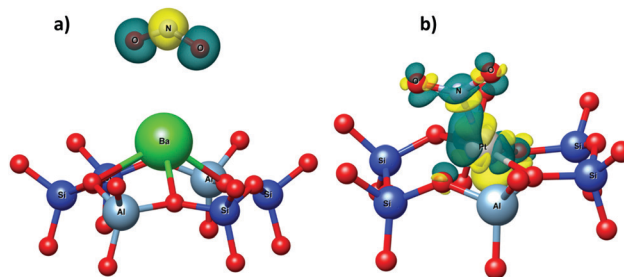


Fig. 6 Iso-surface electron density for NO<sub>2</sub> interaction with Ba-FAU (a), and for the most stable configuration of NO<sub>2</sub> interaction with Pt-FAU (b). Yellow and blue colors stand for the negative and positive iso-surfaces mapped from  $+0.003$  to  $-0.003 \text{ electron \AA}^{-3}$ , respectively.

and copper show the lowest interaction values of  $-42$  and  $-27 \text{ kJ mol}^{-1}$  with NO<sub>2</sub>, respectively.

Benco<sup>79</sup> used DFT to study the adsorption of a set of diatomic and triatomic probe molecules on [Zn-Zn]<sup>2+</sup> particles in a ferrierite zeolite. NO and H<sub>2</sub>O molecules were found to interact with a single Zn atom, resulting in interaction energies of  $-48.8$  and  $-100 \text{ kJ mol}^{-1}$ , respectively, very similar to our findings (Table 3). However, the NO<sub>2</sub> molecule was found to interact with both Zn atoms of the [Zn-Zn]<sup>2+</sup> particle, indicating the  $54 \text{ kJ mol}^{-1}$  higher adsorption as compared to our results.

Pt<sup>2+</sup> and Pd<sup>2+</sup> are the only cations that interact with NO<sub>2</sub> through its nitrogen atom and, thus again, they revealed the highest adsorption values of  $-84.7$  and  $-74.2 \text{ kJ mol}^{-1}$ , respectively. The corresponding vdW contribution was estimated to  $-15.4 \text{ kJ mol}^{-1}$  for Pt<sup>2+</sup>. The strong interaction of NO<sub>2</sub> with the Pt cation was confirmed by the iso-surface electron density presented in Fig. 6b.

### 3.2.3 Adsorption of H<sub>2</sub>O

#### 3.2.3.1 Alkaline earth metals Be<sup>2+</sup>, Mg<sup>2+</sup>, Ca<sup>2+</sup>, Sr<sup>2+</sup>, and Ba<sup>2+</sup>.

As shown by their high interaction energy with water around  $-98 \text{ kJ mol}^{-1}$  (Table 3), all studied cations display a high affinity for this guest, with a vdW contribution of 9%. According to the HSAB theory,<sup>78</sup> alkaline earth metals are considered as hard acids, showing a high affinity for hard bases such as H<sub>2</sub>O, which is confirmed by the iso-surface electron density (Fig. 7a). These results are in accordance with the theoretical work of Benco and Tunega<sup>69</sup> on mordenite.

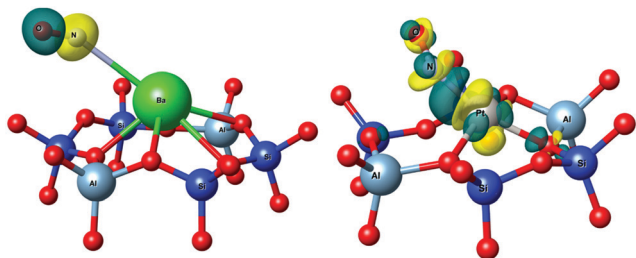


Fig. 5 Iso-surface electron density for two cations: first, with a weak interaction energy between Ba<sup>2+</sup> and NO and second with a strong interaction energy between Pt<sup>2+</sup> and NO. Yellow and blue colors represent the negative and positive iso-surfaces corresponding to  $+0.003$  and  $-0.003 \text{ electron \AA}^{-3}$ , respectively.

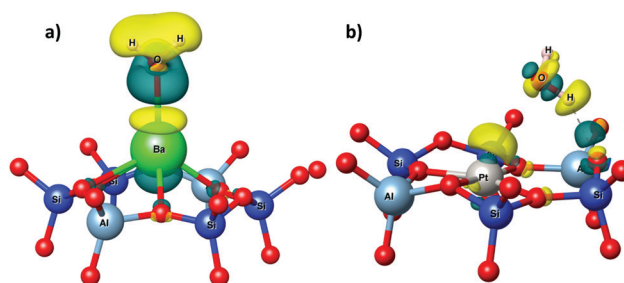


Fig. 7 Iso-surface electron density for the most stable configuration of water adsorption on Ba-FAU (a) and Pt-FAU (b). Yellow and green colors represent the negative and positive iso-surfaces corresponding to  $+0.003$  and  $-0.003 \text{ electron \AA}^{-3}$ , respectively.



**3.2.3.2 Transition metals  $\text{Zn}^{2+}$ ,  $\text{Fe}^{2+}$ ,  $\text{Cu}^{2+}$ ,  $\text{Pd}^{2+}$  and  $\text{Pt}^{2+}$ .** With interaction values of  $-105.3 \text{ kJ mol}^{-1}$  and  $-81.6 \text{ kJ mol}^{-1}$ ,  $\text{Zn}^{2+}$  and  $\text{Cu}^{2+}$  display the strongest interactions with water (Table 3). These values are close to those calculated for alkaline earth metals (Table 3). Considering the HSAB theory,  $\text{Zn}^{2+}$  and  $\text{Cu}^{2+}$  are the hardest acids amongst all transition metals tested.

On the other hand,  $\text{Pd}^{2+}$  and  $\text{Pt}^{2+}$  exhibit weak interactions with water as indicated by the low interaction energies observed, of  $-48.2 \text{ kJ mol}^{-1}$  and  $-33.2 \text{ kJ mol}^{-1}$ , respectively. Indeed, located below  $\text{Zn}^{2+}$  and  $\text{Cu}^{2+}$  in the periodic table,  $\text{Pd}^{2+}$  and  $\text{Pt}^{2+}$  are softer cations. The iso-surface electron-density representation (Fig. 7b) confirms the weak interaction between Pt and water.

Recently, Mandal *et al.*<sup>80</sup> provided insights into the molecular structure of Pd cations in SSZ-13 zeolites and their interaction with  $\text{H}_2\text{O}$  and NO using experimental and computational analyses. The most stable position of Pd was found to be equal to the site II used here (Fig. 1), in which the six-membered ring has two aluminum atoms on opposite sides. Once again, the interaction energies of  $-42$  and  $-123 \text{ kJ mol}^{-1}$  for  $\text{H}_2\text{O}$  and  $\text{NO}_2$  molecules, respectively, agree with the values listed in Table 3.

### 3.3. Selection of the most effective cation to selectively capture $\text{NO}_x$

**3.3.1 Thermodynamic selectivity of cation-exchanged faujasites.** Here, our objective was to identify the most effective charge-compensating cation for the selective trapping of  $\text{NO}_x$  in the presence of water by comparing the interaction energies of NO,  $\text{NO}_2$  and  $\text{H}_2\text{O}$  in the different cation-exchanged faujasite zeolites (Fig. 8). Knowing that, in diesel exhaust gas, the concentrations of  $\text{NO}_x$  (300–1000 ppm)<sup>8,9</sup> are much lower than those of water (10 000 ppm),<sup>81</sup> the adsorbent will have to show a much higher affinity for NO and  $\text{NO}_2$  than for water.

$\text{Be}^{2+}$ ,  $\text{Mg}^{2+}$ ,  $\text{Ca}^{2+}$ ,  $\text{Sr}^{2+}$ ,  $\text{Ba}^{2+}$ ,  $\text{Zn}^{2+}$ , and  $\text{Cu}^{2+}$ -exchanged FAUs exhibit a higher or equivalent affinity for water than that for  $\text{NO}_x$  (Fig. 8). NO and  $\text{NO}_2$  have almost the same interaction energy on a given cation, and their interaction decreases in absolute value from  $\text{Mg}^{2+}$  ( $49 \text{ kJ mol}^{-1}$ ) to  $\text{Ba}^{2+}$  ( $23.5 \text{ kJ mol}^{-1}$ ). This indicates that these materials will be poor sorbents

for  $\text{NO}_x$  and unsuitable for the intended pollution control application.

As shown in Fig. 8,  $\text{Fe}^{2+}$ -exchanged FAU exhibits a similar affinity for water and  $\text{NO}_2$  ( $-56.3$  and  $-53.7 \text{ kJ mol}^{-1}$ , respectively), but much higher affinity for NO ( $-155 \text{ kJ mol}^{-1}$ ). This means that water is expected to play a detrimental role on  $\text{NO}_2$  adsorption. However, the  $\text{NO}_2$  molecule appears to be highly reactive with water in zeolites, leading to NO formation;<sup>82</sup> therefore,  $\text{Fe}^{2+}$  could be an appropriate cation for selectively trapping  $\text{NO}_x$  in the presence of water owing to its high affinity for NO.

Palladium and platinum are the only cations showing a higher affinity for NO and  $\text{NO}_2$  compared to water (Fig. 8 and Table 3). NO shows a high affinity for both cations ( $-145.6$  and  $-168.7 \text{ kJ mol}^{-1}$ , respectively) followed by  $\text{NO}_2$  ( $-84.7$  and  $-74.2 \text{ kJ mol}^{-1}$ ). These interaction energies are significantly higher than those of water ( $-33.2$  and  $-48.2 \text{ kJ mol}^{-1}$  for  $\text{Pd}^{2+}$  and  $\text{Pt}^{2+}$ , respectively). Therefore, water is not expected to inhibit the adsorption of  $\text{NO}_x$  in these zeolites. These results reveal that in terms of thermodynamic selectivity,  $\text{Pd}^{2+}$ ,  $\text{Pt}^{2+}$  and in a lesser extend  $\text{Fe}^{2+}$  forms are clearly the most interesting faujasites for the selective capture of  $\text{NO}_x$  from water.

**3.3.2 Regeneration of the faujasites.** One further requirement of the adsorbent is to prevent chemical reactions and by-product development that would limit the reliability of the trapping process and the regeneration of the sorbent.<sup>83,84</sup> This can be performed by a full comparative analysis of bond lengths before and after adsorption, and the less the bond is activated (*i.e.*, stretched) the more the cation-faujasite is efficient for our purpose.

For alkaline earth cations, the bond length analysis for the pristine and loaded faujasites (Fig. 9) revealed that the NO bond length slightly decreases (from  $0.006$  to  $0.008 \text{ \AA}$  for most cations). The “N–O1” bond length with the first oxygen atom in  $\text{NO}_2$  is almost unaffected but the “N–O2” bond with the second oxygen is stretched with an average variation of  $0.02 \text{ \AA}$ . Concerning  $\text{H}_2\text{O}$ , the distances of the two water bonds (O–H) are barely changed. In terms of regeneration, alkaline earth cations can safely be used for NO removal. However,  $\text{NO}_2$  may develop undesirable by-product formation by chemically reacting with these cations and other molecules. One additional observation in Fig. 9 is that beryllium has the most noticeable differences in bond lengths (both stretched and retracted); this may be attributed to its small ionic radius (Table 1). Therefore, we can suggest that the smaller the radius, the higher the probability of activating the bond length becomes.

Looking at transition metals, all five cations can be safely used to trap NO, as their (N–O) bond lengths become shorter than those in the gas phase (Fig. 9). For  $\text{NO}_2$ , the significant activation of both N–O1 and N–O2 bonds occurs for  $\text{Fe}^{2+}$ ,  $\text{Cu}^{2+}$  and  $\text{Zn}^{2+}$ , while only a slight variation in the bond length from  $0.004$  and  $0.005 \text{ \AA}$  is observed for  $\text{Pd}^{2+}$  and  $\text{Pt}^{2+}$ , respectively. These variations are too small for affecting the regeneration process and are therefore negligible. Concerning water adsorption, a minor variation in the H–O bond length was observed

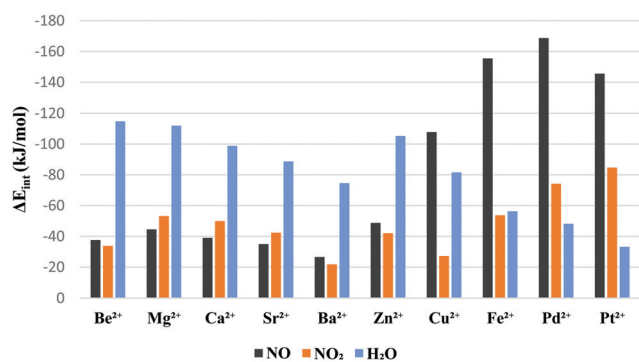


Fig. 8 Total interaction energies of NO,  $\text{NO}_2$ , and  $\text{H}_2\text{O}$  with divalent cation-exchanged faujasites, calculated using the PBE + TS/HI level of theory.



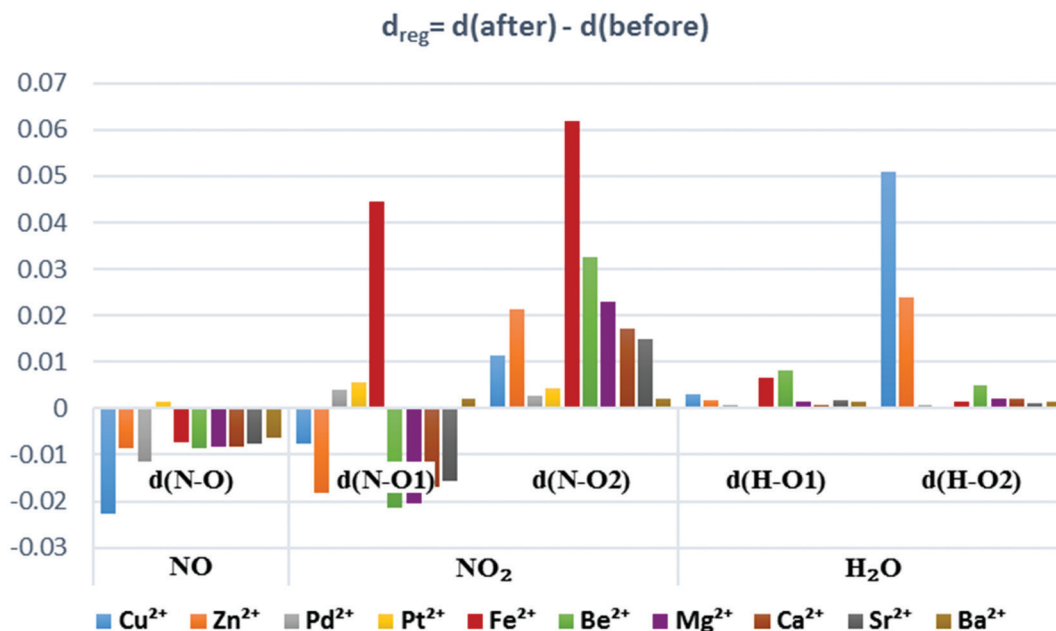


Fig. 9 Variation of the bond lengths of molecules between the gas phase and once adsorbed in faujasites. N–O (in the NO molecule), N–O1 with the first oxygen atom, and N–O2 with the second oxygen atom (in the NO<sub>2</sub> molecule) and O–H1 and O–H2 (in water).

for all cations, except for zinc and copper where the variation in the O–H bond of water was significant (Fig. 9).

Indeed, the analysis of the bond activation shows that only Pd<sup>2+</sup> and Pt<sup>2+</sup> can be effectively used for NO<sub>x</sub> trapping. In the following, we will evaluate the potential of Pt<sup>2+</sup>, which is less costly than Pd<sup>2+</sup>, when embedded in a realistic faujasite Y structure characterized by a Si/Al ratio of 2.4.

### 3.4. Evaluation of Pt(II)–NaY for NO<sub>x</sub> capture

To obtain a Pt(II)–NaY structure (Si/Al ratio = 2.4), 14 Si atoms were substituted by 14 Al atoms in the primitive cell (Fig. 10). The distribution of platinum cations in the zeolitic Y-structure may have an impact on the adsorption mechanisms of NO<sub>x</sub>. Numerous experimental and, more recently, simulation methods have been reported on the location of cations in the faujasite. Frising and Leflaive<sup>47</sup> have gathered and presented in an extensive

review, all the different results that have been published in the literature over the years.

For platinum, only one reference was found where the Na–Y zeolite was partially Pt-exchanged.<sup>85</sup> Therefore, the molecular formula of the investigated cell is Pt<sub>4</sub>Na<sub>6</sub>Al<sub>14</sub>Si<sub>34</sub>O<sub>96</sub>. In this cell, unexchanged Na<sup>+</sup> cations seem to prefer site II (supercage) followed by site I (at the center of the hexagonal prism), while Pt<sup>2+</sup> cations tend to occupy site II and site I' (in the sodalite cage) (Fig. 10).

**3.4.1 Thermodynamic selectivity of cation-exchanged faujasites.** The interaction energies calculated for NO, NO<sub>2</sub> and H<sub>2</sub>O in Pt–Y zeolites (Fig. 11) follow the same trend that presented above for USY (Fig. 8). NO<sub>x</sub> molecules interact strongly with the zeolite with associated interaction energies of  $-269.0 \text{ kJ mol}^{-1}$  and  $-199.8 \text{ kJ mol}^{-1}$  for NO and NO<sub>2</sub>, respectively, which are higher than the value obtained for H<sub>2</sub>O ( $-38.4 \text{ kJ mol}^{-1}$ ). Therefore, upon increasing the Pt concentration

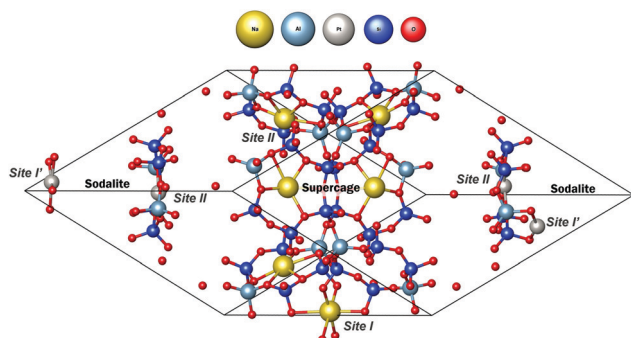


Fig. 10 The Pt–NaY zeolite primitive cell displayed in balls and stick cells, with three accessible sites. Site II (supercage), site I (hexagonal prism) and site I' (sodalite cage).

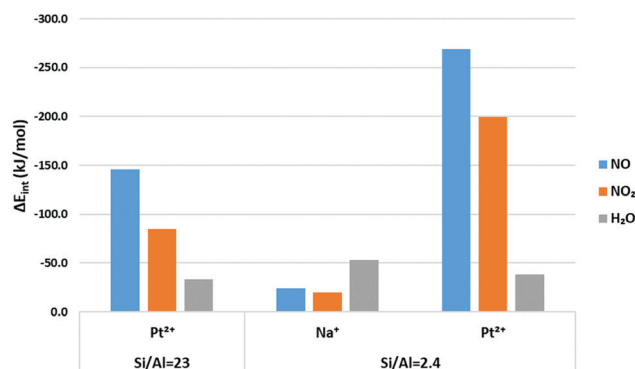


Fig. 11 Total interaction energies of NO, NO<sub>2</sub>, and H<sub>2</sub>O with platinum exchanged Na–Y zeolites, calculated using the PBE + TS/HI level of theory.





(i.e., Si/Al ratio = 2.4), the affinity towards  $\text{NO}_x$  molecules is enhanced, while the adsorption of water molecule shows no change related to the concentration of the cation.

By contrast, the difference in interaction energies of  $\text{NO}_x$  with increasing the cation concentration is surprisingly relatively high, especially since in both cases the adsorption takes place on the same cation position (site II). These observations tend to be driven by the location stability of the cation.

Comparing the [Pt–O] distance between the Pt(II) cation and the D6R oxygens on both Si/Al ratios, it was found that, for the pristine bare zeolite, the platinum cation located on the D6R plane binds strongly to four oxygens, with an average distance of 2.07 Å. Upon adsorption, Pt on zeolite Y was found to be more sensitive to  $\text{NO}_x$  adsorption. The platinum in zeolite Y is displaced from its original position and slightly elevated from the D6R plane with 2.04 Å (Fig. 13e and f) compared to 1.08 Å for USY (Fig. 5).

This higher mobility of the Pt cations in zeolite Y compared to zeolite USY seems to be related to the influence of neighboring cations in the sodalite cage. As shown in Fig. 12, the sodalite cage is strongly perturbed upon  $\text{NO}_x$  adsorption, and the site II Pt cation is pulled out from its original position, subsequently followed by a displacement of the site I' Pt cation towards this vacant site II. This cation confinement effect leads to a greater exposure of the site II Pt cation to the probe molecule compared to the USY zeolite.

The migration of cations from site II to the supercage in zeolite Y has been discussed in many studies: Typically, some of us<sup>86</sup> demonstrated by molecular dynamics combined with complex impedance spectroscopy measurements that methanol perturbs the Na–Y zeolite, moving cations from site II to the center of the supercage, followed by hopping of SI' cations from the sodalite cage into the supercage to fill the vacant SII sites. Klier<sup>87</sup> also mentioned that a CO molecule induces the displacement of Cu(I) from less accessible to more accessible positions in Y-type zeolites.

As a result, this leads to a higher interaction energy along with 0.21 and 0.19 |e| charge transfer (eqn (4)) for Pt–NO and

Pt– $\text{NO}_2$ , respectively (Fig. 13e and f), compared to 0.14 and 0.09 |e| (eqn (4)) found previously for the USY zeolite. In contrast, a slight perturbation of the Pt position is observed upon  $\text{H}_2\text{O}$  adsorption, demonstrating the low interaction energy and a charge transfer of 0.05 |e| (eqn (4)) (Fig. 13g).

Similarly, the presence of residual sodium from the partially exchanged zeolite may affect our  $\text{NO}_x$  trapping and should therefore be investigated. Adsorption of  $\text{NO}_x$  on these cations revealed very low interaction energies of  $-24$  and  $-20 \text{ kJ mol}^{-1}$  for NO and  $\text{NO}_2$ , respectively (Fig. 11). While a strong affinity towards water has been achieved at an interaction energy of  $-55 \text{ kJ mol}^{-1}$  (Fig. 11), in agreement with the HSAB principle.<sup>78</sup> These results indicate that the  $\text{NO}_x$  trapping efficiency would be improved in tandem with a high Pt exchange in the Na–Y zeolite.

The reported high  $\text{NO}_x$  interaction energies with Pt cations along with the low interaction energies for Na cations can be understood by studying the differences in the electron density ( $\Delta\rho$ ) induced by adsorption. In this context, we found that the interactions between N and Pt atoms display a significant electron transfer (Fig. 13e and f), the green density around the  $\text{NO}_x$  molecules reflecting the loss of charges towards the yellow area of the Pt cation. For Na cations, a poor charge transfer can be observed upon adsorption of  $\text{NO}_x$  (Fig. 13a and b), and the water molecule, however, showed a higher charge transfer but mainly in the form of hydrogen bonding with the D6R oxygen atom (Fig. 13c).

**3.4.2 Regeneration of Pt(II)–NaY faujasites.** A comprehensive comparative analysis of the bond lengths of the pristine and loaded zeolites has been achieved.

For USY (Fig. 4a), the NO molecule was found to be adsorbed by its nitrogen atom on the Y zeolite (Fig. 13e). This adsorption configuration maintained the same bond length, preventing it from activation (Fig. 14), similarly to what has been observed on USY (Fig. 9).

For  $\text{NO}_2$ , due to the large displacement of the cation position,  $\pi$  interactions were observed between the Pt of the Y zeolite and the molecule (Fig. 13f). This adsorption configuration led to a

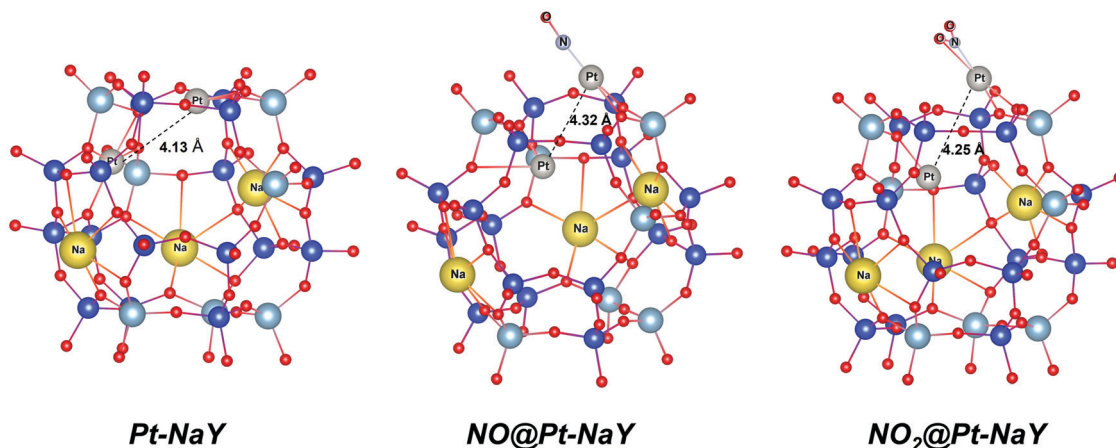


Fig. 12 Displacement of site I' and site II Pt cations upon  $\text{NO}_x$  adsorption in Y-type zeolites.



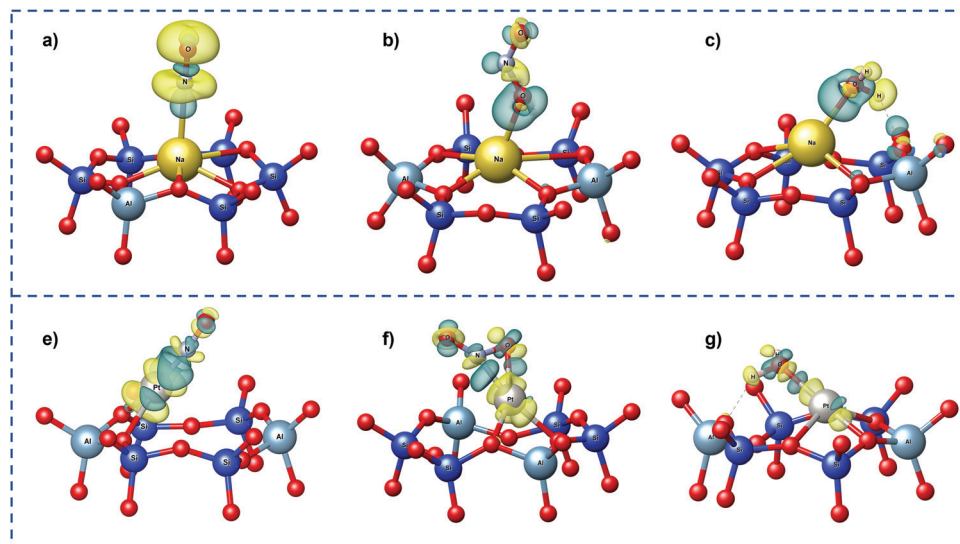


Fig. 13 Iso-surface electron density for the most stable configurations of NO, NO<sub>2</sub> and H<sub>2</sub>O adsorption on Na-Y (a–c) and Pt-NaY (e–g) zeolites. Yellow and green colors represent the negative and positive iso-surfaces corresponding to +0.01/+0.003 and –0.01/–0.003 electron Å<sup>–3</sup> for Pt and Na, respectively.

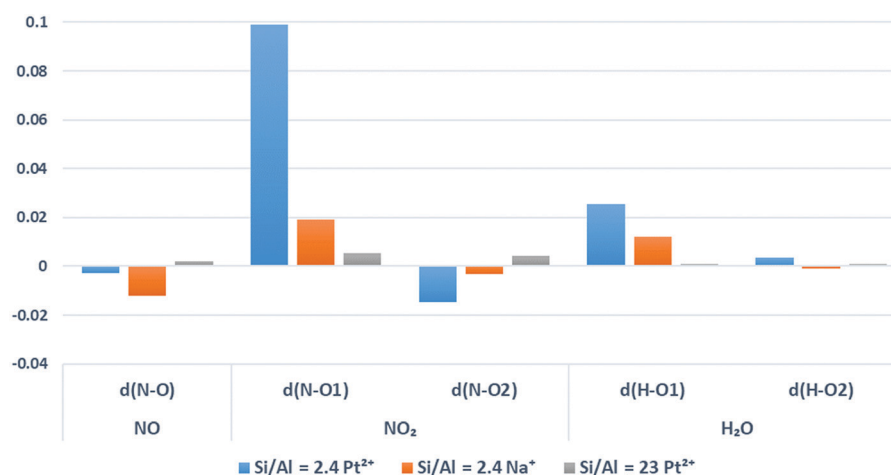


Fig. 14 Variation of the bond lengths of the molecules before the adsorption on cation-exchange faujasites (gas phase) and after the adsorption. N–O (in the NO molecule), N–O1 with the first oxygen atom, and N–O2 with the second oxygen atom (in the NO<sub>2</sub> molecule) and O–H1 and O–H2 (in water).

significant stretching of the non-interactive (N–O) bond (Fig. 14). In contrast, for USY, the NO<sub>2</sub> molecule was adsorbed only *via* its nitrogen (Fig. 4b), resulting in no change in its bond length (Fig. 14).

Concerning water, due to the weak hydrogen bonding that occurred during adsorption (Fig. 13g), the bond length of the molecule was negligibly stretched (Fig. 14).

To summarize, the binding analysis shows that Pt(II)–NaY can be safely used for NO removal in the presence of water. However, because of the significant increase of NO<sub>2</sub> bond lengths, Pt(II)–NaY appears to be unsuitable for NO<sub>2</sub> removal, as it can lead to the formation of undesirable by-products, resulting from the dissociation and the chemical reaction of NO<sub>2</sub> with platinum and other molecules. In addition, the revealed high interactions between NO<sub>x</sub> and Pt may leave the latter difficult

to regenerate. Therefore, future studies are needed to investigate the desorption properties of the most promising zeolites to determine the optimal regeneration temperature.

## 4. Conclusion

In summary, in the context of the prevention of harmful emissions from diesel engines, DFT simulations using the van der Waals correction have been conducted to study the effect of water on the NO<sub>x</sub> capture by cation containing faujasites. Several divalent cation (alkaline earth metals (Be<sup>2+</sup>, Mg<sup>2+</sup>, Ca<sup>2+</sup>, Sr<sup>2+</sup>, and Ba<sup>2+</sup>) and transition metals (Fe<sup>2+</sup>, Cu<sup>2+</sup>, Zn<sup>2+</sup>, Pd<sup>2+</sup>, and Pt<sup>2+</sup>)) exchanged faujasites were tested to identify the most selective sorbents toward NO and NO<sub>2</sub> contaminants.



Overall, when considering thermodynamic selectivity criteria, our interaction energy calculations show that alkaline earth metals, as well as  $\text{Cu}^{2+}$  and  $\text{Zn}^{2+}$ , exhibit a higher affinity for water than for  $\text{NO}_x$ , indicating their unsuitability for the target application, whereas the remaining charge-compensating cations ( $\text{Fe}^{2+}$ ,  $\text{Pd}^{2+}$  and  $\text{Pt}^{2+}$ ) behave more efficiently, since all of them show a greater affinity for  $\text{NO}$ , leaving water with no expected detrimental effect on  $\text{NO}_x$  adsorption, with the exception of  $\text{Fe}^{2+}$  that presents a similar affinity for water and  $\text{NO}_2$ .

Nevertheless, the bond activation analysis discarded  $\text{Fe}^{2+}$  from the suitable cations list, since a significant activation of the N–O1 and N–O2 bonds is observed for the adsorption of  $\text{NO}_2$  on  $\text{Fe}^{2+}$ , resulting in undesired by-product formation, whereby a negligible variation in the bond length is observed for  $\text{Pd}^{2+}$  and  $\text{Pt}^{2+}$ .

The  $\text{Pt}^{2+}$  cation was then incorporated and studied within the Y zeolite ( $\text{Si}/\text{Al} = 2.4$ ). The results highlight that  $\text{Pt}^{2+}$  faujasite Y is an interesting material for the removal of  $\text{NO}_x$  from diesel engine exhaust.

This screening method transferable to the adsorption study of other contaminants by zeolite sorbents, including ammonia gas and formaldehyde among others, is expected to guide the experimental effort towards the synthesis of the optimum sorbents to avoid tedious and time-consuming trial-error approach.

## Conflicts of interest

There are no conflicts to declare.

## Acknowledgements

This work was granted access to the HPC resources of TGCC under the allocation 2020 A0080910433 made by GENCI. This work was partially funded by the French National Research Agency NOA Project (ANR-20-CE08-0024). AD, AH and MB acknowledge financial support by the Ministry of Europe and Foreign Affairs, the Ministry of Higher Education, Research and Innovation and the French Institute of Rabat (PHC TOUBKAL 2021 (French-Morocco bilateral program) Grant Number: 12345AB). MB also acknowledges financial support through the COMETE project (CONception *in silico* de Matériaux pour l'Environnement et l'Energie) co-funded by the European Union under the program "FEDER-FSE Lorraine et Massif des Vosges 2014–2020".

## References

- 1 S. Gligorovski and J. P. D. Abbatt, An indoor chemical cocktail, *Science*, 2018, **359**, 632–633.
- 2 IARC Working Group on the Evaluation of Carcinogenic Risks to Humans and International Agency for Research on Cancer, *Diesel and gasoline engine exhausts and some nitroaromatics*, 2014.
- 3 9 out of 10 people worldwide breathe polluted air, but more countries are taking action, <https://www.who.int/news/item/02-05-2018-9-out-of-10-people-worldwide-breathe-polluted-air-but-more-countries-are-taking-action>.
- 4 W. Jedrychowski, F. Perera, D. Mrozek-Budzyn, E. Mroz, E. Flak, J. D. Spengler, S. Edwards, R. Jacek, I. Kaim and Z. Skolicki, Gender differences in fetal growth of newborns exposed prenatally to airborne fine particulate matter, *Environ. Res.*, 2009, **109**, 447–456.
- 5 European Environment Agency. and European Topic Centre on Air Pollution and Climate Change Mitigation (ETC/ACM)., Air quality in Europe: 2017 report., Publications Office, LU, 2017.
- 6 A. Kumar Agrawal, S. K. Singh, S. Sinha and M. K. Shukla, Effect of EGR on the exhaust gas temperature and exhaust opacity in compression ignition engines, *Sadhana*, 2004, **29**, 275–284.
- 7 H. Ahari, M. Smith, M. Zammit, K. Price, J. Jacques, T. Pauly and L. Wang, Impact of SCR Integration on  $\text{N}_2\text{O}$  Emissions in Diesel Application, *SAE Int. J. Passeng. Cars - Mech. Syst.*, 2015, **8**, 526–530.
- 8 X. Wang, D. Westerdahl, J. Hu, Y. Wu, H. Yin, X. Pan and K. Max Zhang, On-road diesel vehicle emission factors for nitrogen oxides and black carbon in two Chinese cities, *Atmos. Environ.*, 2012, **46**, 45–55.
- 9 T. Lee, J. Park, S. Kwon, J. Lee and J. Kim, Variability in operation-based  $\text{NO}_x$  emission factors with different test routes, and its effects on the real-driving emissions of light diesel vehicles, *Sci. Total Environ.*, 2013, **461–462**, 377–385.
- 10 AVIS et RAPPORT de l'Anses relatif à l'Evaluation des méthodes de mesure de 27 substances listées en annexe de la directive (UE) n°2017/164 de la Commission du 31 janvier 2017 | Anses - Agence nationale de sécurité sanitaire de l'alimentation, de l'environnement et du travail, <https://www.anses.fr/fr/content/avis-et-rapport-de-l-anses-relatif-a-l-evaluation-des-methodes-de-mesure-de-27-substances>.
- 11 L. Castoldi, L. Lietti, R. Bonzi, N. Artioli, P. Forzatti, S. Morandi and G. Ghiotti, The  $\text{NO}_x$  Reduction by CO on a Pt–K/Al<sub>2</sub>O<sub>3</sub> Lean  $\text{NO}_x$  Trap Catalyst, *J. Phys. Chem. C*, 2011, **115**, 1277–1286.
- 12 J.-K. Lai and I. E. Wachs, A Perspective on the Selective Catalytic Reduction (SCR) of NO with  $\text{NH}_3$  by Supported V<sub>2</sub>O<sub>5</sub>–WO<sub>3</sub>/TiO<sub>2</sub> Catalysts, *ACS Catal.*, 2018, **8**, 6537–6551.
- 13 G. Centi and S. Perathoner, Nature of active species in copper-based catalysts and their chemistry of transformation of nitrogen oxides, *Appl. Catal., A*, 1995, **132**, 179–259.
- 14 Z. G. Liu, D. R. Berg, T. A. Swor and J. J. Schauer, Comparative Analysis on the Effects of Diesel Particulate Filter and Selective Catalytic Reduction Systems on a Wide Spectrum of Chemical Species Emissions, *Environ. Sci. Technol.*, 2008, **42**, 6080–6085.
- 15 J. Y. Yan, G.-D. Lei, W. M. H. Sachtler and H. H. Kung, Deactivation of Cu/ZSM-5 Catalysts for Lean  $\text{NO}_x$  Reduction: Characterization of Changes of Cu State and Zeolite Support, *J. Catal.*, 1996, **161**, 43–54.
- 16 F. Delachaux, C. Vallières, H. Monnier and M.-T. Lecler, Experimental study of NO and  $\text{NO}_2$  adsorption on a fresh or



- dried NaY zeolite: influence of the gas composition by breakthrough curves measurements, *Adsorption*, 2019, **25**, 95–103.
- 17 O. Monticelli, R. Loenders, P. A. Jacobs and J. A. Martens, NO<sub>x</sub> removal from exhaust gas from lean burn internal combustion engines through adsorption on FAU type zeolites cation exchanged with alkali metals and alkaline earth metals, *Appl. Catal., B*, 1999, **21**, 215–220.
  - 18 A. Sultana, R. Loenders, O. Monticelli, C. Kirschhock, P. A. Jacobs and J. A. Martens, DeNO<sub>x</sub> of Exhaust Gas from Lean-Burn Engines through Reversible Adsorption of N<sub>2</sub>O<sub>3</sub> in Alkali Metal Cation Exchanged Faujasite-Type Zeolites, *Angew. Chem., Int. Ed.*, 2000, **39**, 2934–2937.
  - 19 IZA Structure Commission, <https://www.iza-structure.org/>.
  - 20 S. Sircar and A. L. Myers, *Handbook of Zeolite Science and Technology Chapter 22 Gas Separation by Zeolites*, CRC Press, 2003, DOI: [10.1201/9780203911167](https://doi.org/10.1201/9780203911167).
  - 21 P. A. Jacobs, E. M. Flanigen, J. C. Jansen and H. van Bekkum, *Introduction to Zeolite Science and Practice*, Elsevier Science, 2001.
  - 22 M. Guisnet and J.-P. Gilson, *Zeolites for Cleaner Technologies*, Catalytic Science Series, Volume 3. Series Edited by Graham J. Hutchings (Cardiff University), Imperial College Press, London, 2002, ISBN 1-86094-329-2, *J. Am. Chem. Soc.*, 2003, **125**, 6839.
  - 23 W. M. Meier, The crystal structure of mordenite (ptilolite), *Z. Kristallogr. - Cryst. Mater.*, 1961, **115**, 439–450.
  - 24 R. J. Argauer and G. R. Landolt, Crystalline zeolite zsm-5 and method of preparing the same, *US Pat.*, US3702886A, 1972.
  - 25 C. Baerlocher, L. B. McCusker and D. H. Olson, *Atlas of Zeolite Framework Types*, Elsevier, 2007.
  - 26 E. P. Hessou, W. G. Kanhounon, D. Rocca, H. Monnier, C. Vallières, M. Badawi and S. Lebègue, Adsorption of NO, NO<sub>2</sub>, CO, H<sub>2</sub>O and CO<sub>2</sub> over isolated monovalent cations in faujasite zeolite: a periodic DFT investigation, *Theor. Chem. Acc.*, 2018, **137**, 161.
  - 27 C. R. A. Catlow, B. Smit and R. A. van Santen, *Computer Modelling of Microporous Materials*, Elsevier, 2004.
  - 28 T. Ayadi, M. Badawi, L. Cantrel and S. Lebègue, Rational approach for an optimized formulation of silver-exchanged zeolites for iodine capture from first-principles calculations, *Mol. Syst. Des. Eng.*, 2022, **7**(5), 422–433.
  - 29 M. Chebbi, S. Chibani, J.-F. Paul, L. Cantrel and M. Badawi, Evaluation of volatile iodine trapping in presence of contaminants A periodic DFT study on cation exchanged-faujasite, *Microporous Mesoporous Mater.*, 2017, **239**, 111–122.
  - 30 G. D. Pirngruber, P. Raybaud, Y. Belmabkhout, J. Čejka and A. Zukal, The role of the extra-framework cations in the adsorption of CO<sub>2</sub> on faujasite Y, *Phys. Chem. Chem. Phys.*, 2010, **12**, 13534–13546.
  - 31 I. Khalil, H. Jabraoui, S. Lebègue, W. J. Kim, L.-J. Aguilera, K. Thomas, F. Maugé and M. Badawi, Biofuel purification: Coupling experimental and theoretical investigations for efficient separation of phenol from aromatics by zeolites, *Chem. Eng. J.*, 2020, **402**, 126264.
  - 32 H. Jabraoui, I. Khalil, S. Lebègue and M. Badawi, Ab initio screening of cation-exchanged zeolites for biofuel purification, *Mol. Syst. Des. Eng.*, 2019, **4**, 882–892.
  - 33 G. Li, S. C. Larsen and V. H. Grassian, Catalytic reduction of NO<sub>2</sub> in nanocrystalline NaY zeolite, *J. Mol. Catal. A: Chem.*, 2005, **227**, 25–35.
  - 34 J. Szanyi, J. H. Kwak and C. H. F. Peden, The Effect of Water on the Adsorption of NO<sub>2</sub> in Na- and Ba-Y, FAU Zeolites: A Combined FTIR and TPD Investigation, *J. Phys. Chem. B*, 2004, **108**, 3746–3753.
  - 35 W. Lutz, Zeolite Y: Synthesis, Modification, and Properties—A Case Revisited, *Adv. Mater. Sci. Eng.*, 2014, **2014**, e724248.
  - 36 D. W. Breck, Crystalline zeolite Y, *US Pat.*, US3130007A, 1964.
  - 37 E. P. Hessou, H. Jabraoui, I. Khalil, M.-A. Dziurla and M. Badawi, Ab initio screening of zeolite Y formulations for efficient adsorption of thiophene in presence of benzene, *Appl. Surf. Sci.*, 2021, **541**, 148515.
  - 38 M. U. C. Braga, G. H. Perin, L. H. de Oliveira and P. A. Arroyo, DFT calculations for adsorption of H<sub>2</sub>S and other natural gas compounds on (Fe, Co, Ni, Cu and Zn)-Y zeolite clusters, *Microporous Mesoporous Mater.*, 2022, **331**, 111643.
  - 39 A. A. Costa, P. R. S. Braga, J. L. de Macedo, J. A. Dias and S. C. L. Dias, Structural effects of WO<sub>3</sub> incorporation on USY zeolite and application to free fatty acids esterification, *Microporous Mesoporous Mater.*, 2012, **147**, 142–148.
  - 40 L. Cao, F. Xu, Y.-Y. Liang and H.-L. Li, Preparation of the Novel Nanocomposite Co(OH)<sub>2</sub>/Ultra-Stable Y Zeolite and Its Application as a Supercapacitor with High Energy Density, *Adv. Mater.*, 2004, **16**, 1853–1857.
  - 41 K. O. Sulaiman, M. Sajid and K. Alhooshani, Application of porous membrane bag enclosed alkaline treated Y-Zeolite for removal of heavy metal ions from water, *Microchem. J.*, 2020, **152**, 104289.
  - 42 Database of Zeolite Structures, <https://www.iza-structure.org/databases/>.
  - 43 W. H. Baur, On the cation and water positions in faujasite, *Am. Mineral.*, 1964, **49**, 697–704.
  - 44 E. Dempsey, G. H. Kuehl and D. H. Olson, Variation of the lattice parameter with aluminum content in synthetic sodium faujasites. Evidence for ordering of the framework ions, *J. Phys. Chem.*, 1969, **73**, 387–390.
  - 45 F. Porcher, M. Souhassou, Y. Dusaosoy and C. Lecomte, The crystal structure of a low-silica dehydrated NaX zeolite, *Eur. J. Mineral.*, 1999, 333–344.
  - 46 W. Loewenstein, The distribution of aluminum in the tetrahedra of silicates and aluminates, *Am. Mineral.*, 1954, **39**, 92–96.
  - 47 T. Frising and P. Leflaive, Extraframework cation distributions in X and Y faujasite zeolites: A review, *Microporous Mesoporous Mater.*, 2008, **114**, 27–63.
  - 48 S. Buttefey, A. Boutin, C. Mellot-Draznieks and A. H. Fuchs, A Simple Model for Predicting the Na<sup>+</sup> Distribution in Anhydrous NaY and NaX Zeolites, *J. Phys. Chem. B*, 2001, **105**, 9569–9575.





- 49 Z. Nour, D. Berthomieu, Q. Yang and G. Maurin, A Computational Exploration of the CO Adsorption in Cation-Exchanged Faujasites, *J. Phys. Chem. C*, 2012, **116**, 24512–24521.
- 50 H. V. Thang, L. Grajciar, P. Nachtigall, O. Bludský, C. O. Areán, E. Frýdová and R. Bulánek, Adsorption of CO<sub>2</sub> in FAU zeolites: Effect of zeolite composition, *Catal. Today*, 2014, **227**, 50–56.
- 51 P. Kumar, C.-Y. Sung, O. Muraza, M. Cococcioni, S. Al Hashimi, A. McCormick and M. Tsapatsis, H<sub>2</sub>S adsorption by Ag and Cu ion exchanged faujasites, *Microporous Mesoporous Mater.*, 2011, **146**, 127–133.
- 52 C.-Y. Sung, S. Al Hashimi, A. McCormick, M. Tsapatsis and M. Cococcioni, Density Functional Theory Study on the Adsorption of H<sub>2</sub>S and Other Claus Process Tail Gas Components on Copper- and Silver-Exchanged Y Zeolites, *J. Phys. Chem. C*, 2012, **116**, 3561–3575.
- 53 P. Hohenberg and W. Kohn, Inhomogeneous Electron Gas, *Phys. Rev.*, 1964, **136**, B864–B871.
- 54 W. Kohn and L. J. Sham, Self-Consistent Equations Including Exchange and Correlation Effects, *Phys. Rev.*, 1965, **140**, A1133–A1138.
- 55 G. Kresse and J. Hafner, {Ab initio} molecular dynamics for liquid metals, *Phys. Rev. B: Condens. Matter Mater. Phys.*, 1993, **47**, 558–561.
- 56 J. P. Perdew, K. Burke and M. Ernzerhof, Generalized Gradient Approximation Made Simple, *Phys. Rev. Lett.*, 1996, **77**, 3865–3868.
- 57 P. E. Blöchl, Projector augmented-wave method, *Phys. Rev. B: Condens. Matter Mater. Phys.*, 1994, **50**, 17953–17979.
- 58 G. Kresse and D. Joubert, From ultrasoft pseudopotentials to the projector augmented-wave method, *Phys. Rev. B: Condens. Matter Mater. Phys.*, 1999, **59**, 1758–1775.
- 59 G. Kresse and J. Furthmüller, Efficient iterative schemes for ab initio total-energy calculations using a plane-wave basis set, *Phys. Rev. B: Condens. Matter Mater. Phys.*, 1996, **54**, 11169–11186.
- 60 S. Chibani, M. Chebbi, S. Lebègue, T. Bučko and M. Badawi, A DFT investigation of the adsorption of iodine compounds and water in H-, Na-, Ag-, and Cu- mordenite, *J. Chem. Phys.*, 2016, **144**, 244705.
- 61 T. Bučko, S. Lebègue, J. G. Ángyán and J. Hafner, Extending the applicability of the Tkatchenko-Scheffler dispersion correction via iterative Hirshfeld partitioning, *Chem. Phys.*, 2014, **141**, 034114.
- 62 T. Bučko, S. Lebègue, J. Hafner and J. G. Ángyán, Improved Density Dependent Correction for the Description of London Dispersion Forces, *J. Chem. Theory Comput.*, 2013, **9**, 4293–4299.
- 63 T. Bučko, S. Lebègue, J. Hafner and J. G. Ángyán, Tkatchenko-Scheffler van der Waals correction method with and without self-consistent screening applied to solids, *Phys. Rev. B: Condens. Matter Mater. Phys.*, 2013, **87**, 064110.
- 64 A. Tkatchenko and M. Scheffler, Accurate Molecular van der Waals Interactions from Ground-State Electron Density and Free-Atom Reference Data, *Phys. Rev. Lett.*, 2009, **102**, 073005.
- 65 A. G. Petukhov, I. I. Mazin, L. Chioncel and A. I. Lichtenstein, Correlated metals and the  $\{LDA\} + U$  method, *Phys. Rev. B: Condens. Matter Mater. Phys.*, 2003, **67**, 153106.
- 66 W. Tang, E. Sanville and G. Henkelman, A grid-based Bader analysis algorithm without lattice bias, *J. Phys.: Condens. Matter*, 2009, **21**, 084204.
- 67 E. Sanville, S. D. Kenny, R. Smith and G. Henkelman, Improved grid-based algorithm for Bader charge allocation, *J. Comput. Chem.*, 2007, **28**, 899–908.
- 68 G. Henkelman, A. Arnaldsson and H. Jónsson, A fast and robust algorithm for Bader decomposition of charge density, *Comput. Mater. Sci.*, 2006, **36**, 354–360.
- 69 L. Benco and D. Tunega, Adsorption of H<sub>2</sub>O, NH<sub>3</sub> and C<sub>6</sub>H<sub>6</sub> on alkali metal cations in internal surface of mordenite and in external surface of smectite: a DFT study, *Phys. Chem. Miner.*, 2009, **36**, 281–290.
- 70 P. Kozyra, J. Załucka, M. Mitoraj, E. Broclawik and J. Datka, From Electron Density Flow Towards Activation: Benzene Interacting with Cu(I) and Ag(I) Sites in ZSM-5. DFT Modeling, *Catal. Lett.*, 2008, **126**, 241–246.
- 71 T. Kanougi, H. Tsuruya, Y. Oumi, A. Chatterjee, A. Fahmi, M. Kubo and A. Miyamoto, Density functional calculation on the adsorption of nitrogen oxides and water on ion exchanged ZSM-5, *Appl. Surf. Sci.*, 1998, **130–132**, 561–565.
- 72 Y. Wang, Z. Lei, B. Chen, Q. Guo and N. Liu, Adsorption of NO and N<sub>2</sub>O on Fe-BEA and H-BEA zeolites, *Appl. Surf. Sci.*, 2010, **256**, 4042–4047.
- 73 P. Sun, K. Fan, X. Cheng, Z. Qian, Z. Wang, L. Wang and T.-C. Jen, Decoupled NO<sub>x</sub> adsorption and reduction by CO over catalyst Fe/ZSM-5: A DFT study, *Chem. Phys. Lett.*, 2021, **766**, 138344.
- 74 R. Zhang, J. Szanyi, F. Gao and J.-S. McEwen, The interaction of reactants, intermediates and products with Cu ions in Cu-SSZ-13 NH<sub>3</sub> SCR catalysts: an energetic and ab initio X-ray absorption modeling study, *Catal. Sci. Technol.*, 2016, **6**, 5812–5829.
- 75 L. A. M. M. Barbosa, R. A. van Santen and J. Hafner, Stability of Zn(II) Cations in Chabazite Studied by Periodical Density Functional Theory, *J. Am. Chem. Soc.*, 2001, **123**, 4530–4540.
- 76 C. Lamberti, A. Zecchina, E. Groppo and S. Bordiga, Probing the surfaces of heterogeneous catalysts by in situ IR spectroscopy, *Chem. Soc. Rev.*, 2010, **39**, 4951–5001.
- 77 K. I. Hadjiivanov and G. N. Vayssilov, Characterization of oxide surfaces and zeolites by carbon monoxide as an IR probe molecule, *Adv. Catal.*, Academic Press, 2002, vol. 47, pp. 307–511.
- 78 R. G. Pearson, Hard and soft acids and bases, HSAB, part 1: Fundamental principles, *J. Chem. Educ.*, 1968, **45**, 581.
- 79 L. Benco, Adsorption of small molecules on the [Zn-Zn]<sub>2</sub><sup>+</sup> linkage in zeolite. A DFT study of ferrierite, *Surf. Sci.*, 2017, **656**, 115–125.
- 80 K. Mandal, Y. Gu, K. S. Westendorff, S. Li, J. A. Pihl, L. C. Grabow, W. S. Epling and C. Paolucci, Condition-Dependent Pd Speciation and NO Adsorption in Pd/Zeolites, *ACS Catal.*, 2020, **10**, 12801–12818.
- 81 İ. A. Reşitoğlu, K. Altinişik and A. Keskin, The pollutant emissions from diesel-engine vehicles and exhaust after-treatment systems, *Clean Technol. Environ. Policy*, 2015, **17**, 15–27.



- 82 C. Guardiola, J. Martín, B. Pla and P. Bares, Cycle by cycle NO<sub>x</sub> model for diesel engine control, *Appl. Therm. Eng.*, 2017, **110**, 1011–1020.
- 83 M. Brändle and J. Sauer, Combining ab initio techniques with analytical potential functions. A study of zeolite-adsorbate interactions for NH<sub>3</sub> on H-faujasite, *J. Mol. Catal. A: Chem.*, 1997, **119**, 19–33.
- 84 C. Y. Li and L. V. C. Rees, Ion exchange, thermal stability and water desorption studies of faujasites with different Si/Al ratios, *React. Polym., Ion Exch., Sorbents*, 1988, **7**, 89–99.
- 85 P. Gallezot, A. Alarcon-Diaz, J.-A. Dalmon, A. J. Renouprez and B. Imelik, Location and dispersion of platinum in PtY zeolites, *J. Catal.*, 1975, **39**, 334–349.
- 86 G. Maurin, D. Plant, S. Devautour-Vinot, A. Nicolas, F. Henn and J. C. Giuntini, Cation mobility upon adsorption of methanol in NaY faujasite type zeolite: A molecular dynamics study compared to dielectric relaxation experiments, *Eur. Phys. J.: Spec. Top.*, 2007, **141**, 113–116.
- 87 K. Klier, Transition-metal ions in zeolites: the perfect surface sites, *Langmuir*, 1988, **4**, 13–25.

